HHS Public Access

Author manuscript

Science. Author manuscript; available in PMC 2023 February 27.

Published in final edited form as:

Science. 2022 March 11; 375(6585): eabj5861. doi:10.1126/science.abj5861.

Local Connectivity and Synaptic Dynamics in Mouse and Human Neocortex

A full list of authors and affiliations appears at the end of the article.

Abstract

We present a unique, extensive, and open synaptic physiology analysis platform and dataset. Through its application, we reveal principles that relate cell type to synaptic properties and intralaminar circuit organization in the mouse and human cortex. The dynamics of excitatory synapses align with the postsynaptic cell subclass, whereas inhibitory synapse dynamics partly align with presynaptic cell subclass but with considerable overlap. Synaptic properties are heterogeneous in most subclass to subclass connections. The two main axes of heterogeneity are strength and variability. Cell subclasses divide along the variability axis, while the strength axis accounts for significant heterogeneity within the subclass. In the human cortex, excitatory to excitatory synaptic dynamics are distinct from that in the mouse cortex and vary with depth across layers 2 and 3.

Summary Figure:

✟Corresponding author: timj@alleninstitute.org.
†KB present address: KB Cajal Neuroscience, Seattle, WA.
†CT present address: Sandia National Laboratories, Albuquerque, NM
*These authors contributed equally

Author contributions:
Conceptualization: TJ, CK, HZ
Data Curation: LC, SCS, PD, A Ho, CR, LK, JT, CG, DF, AS, WW, NH, Sh Sh, LA, GW, A He, AM, SK, DS, PB, TJ
Formal Analysis: LC, SCS, TC, SI, CT, JG
Methodology: TJ, LC
Investigation: LC, SCS, PD, A Ho, LK, JT, CR, DC, TC, KC, MC, La El, JG, M., JS, HT, KW, KS, MT, TP, DM, AG, KB, TE, Mi Ma, Me Mc, CAP, AR, JB, KB, ND, RE, MG, MH, SDL, KN, RN, LP, SR
Visualization: LC, SCS, TC, SI, CG
Project Administration: FD, Su Su
Resources: RL, TC, ND, CF, MS, CS, BT, MW, MG, TD, CC, RPG., CDK, ALK, JGO, DLS
Software: TB, TJ, LC
Supervision: TJ, JP Lu Es, HZ, EL, GM, Me Mc, ND, RN, St So
Writing - original draft: TJ, LC, SCS, TC, SI, LK, CG
Writing - review & editing: MHK, TH, AA

Competing interests: Authors declare that they have no competing interests.

Supplementary Materials
Materials and Methods
Figs. S1 to S14
Tables S1 to S5
References (78–93)

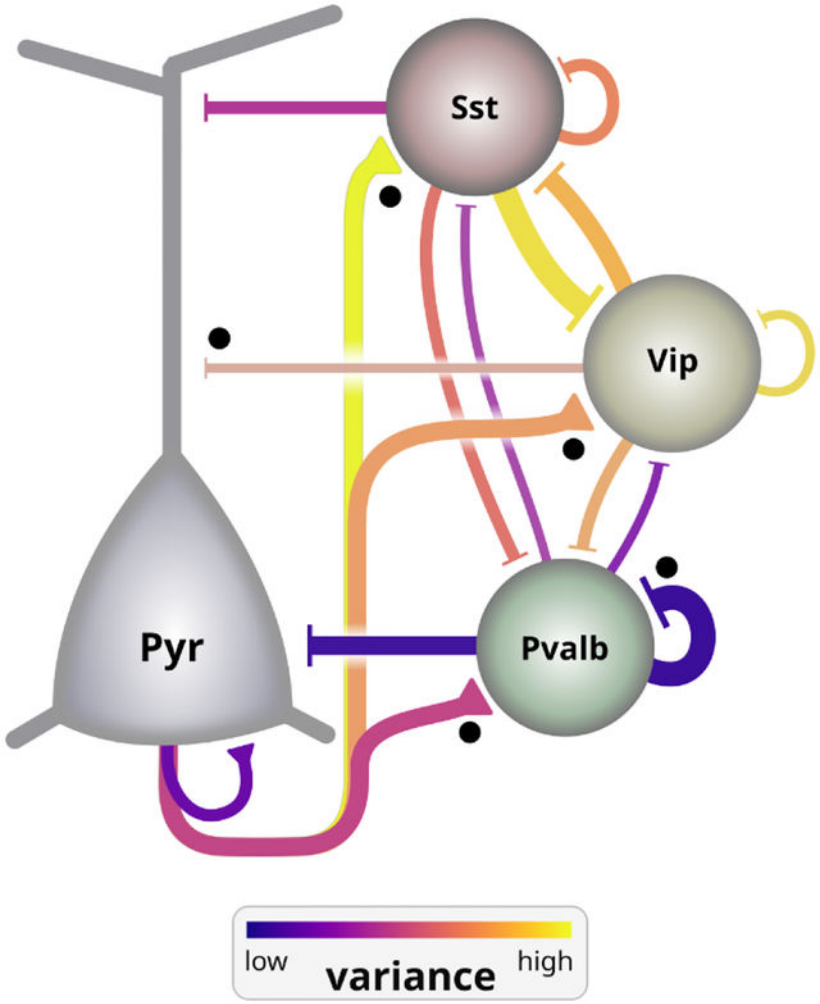

Intralaminar circuit diagram among major excitatory (Pyr) and inhibitory (Pvalb, Sst, Vip) cell subclasses, aggregated from all layers of mouse V1. Line thickness depicts the relative weight (strength and probability of connection) of connections between subclasses. Black dots indicate connections that are stronger in layer 2/3 compared to layer 5. Line color shows the spike-to-spike variance in amplitude of synaptic signaling, which is strongly cell subclass-dependent. Excitatory synapse variance depends on the postsynaptic subclass. Pvalb cells project low variance connections, whereas Sst and Vip project high variance connections.

Summary

The mammalian neocortex is believed to act as the computational substrate for our highest cognitive abilities, particularly the ability to model the world around us and predict the effects of our actions. Many aspects of cortical structure are repeated across brain regions and conserved across species, suggesting a general-purpose approach to cognition. Within this repeating structure, neurons influence the formation of synaptic connections based on their cell type-specific biases. This results in a stereotyped network architecture in which synapse properties and connectivity are strongly influenced by cell type.

Synapses between cell types transmit information in a way that is highly stochastic and depends on the prior history of activity. The dynamic properties of synapses are also strongly dependent on both the pre- and postsynaptic cell types, suggesting an important role in cortical function. This provides a major source of computational diversity that is often absent in neuroscience modeling studies as well as modern machine learning architectures.

Neurons are broadly grouped into excitatory and inhibitory classes, each of which can be divided into more specific subclasses. Cortical inhibitory neurons, for example, are commonly divided into Pvalb, Sst, and Vip subclasses and are distributed broadly across cortical layers. In contrast, most excitatory cell subclasses occupy narrower regions across cortical layers.

Rationale: Understanding the connectivity among cell subclasses and the computations performed at their synapses is an essential step to understanding cortical circuit function. This has led to experiments in different species, brain regions, ages, etc. that focus on one or a few circuit elements. These efforts offer an excellent depth of insight to isolated regions of the circuit but offer a fragmented view of the circuit as a whole. Further, the difficulty of accessing these historical data discourages reuse and reanalysis. We saw an opportunity to expand upon this history and conduct a more comprehensive and standardized survey than has been attempted in the past. By publishing the analyses, tools, and data that characterize cortical connection properties, we encourage a more unified approach to describing cortical function.

Results: We used microelectrodes to record the activity of 1731 synaptic connections across diverse types in living tissue samples from mouse and human neocortex. We characterized these connections with the aid of a synaptic release model and found that excitatory dynamics aligned with postsynaptic cell subclass, whereas inhibitory dynamics aligned with the presynaptic subclass in ways that were subclass-specific. Synaptic variability was a primary driver of these cross-subclass differences in mouse cortex. Compared to mouse, human excitatory connections were tuned toward stability and reliability pointing toward species differences in cortical function. We further introduced a method to estimate the rate of connectivity between cell types that accounts for differences between experimental preparations. With this approach we compared connection probabilities across layer, cell subclass, and species. For instance, connectivity between excitatory cells and Vip inhibitory cells was present in layer 2/3 and absent in layer 5/6 of mouse cortex. Likewise, connection probability among layer 4 excitatory cells was high in mouse cortex and nearly absent in human cortex. Overall, we found that layer-specific circuit representations are necessary to capture the diversity of intralaminar connectivity among cortical cell subclasses.

Conclusion: We have generated a comprehensive dataset describing synaptic connections within each layer in the mouse and human cortex. Our deep characterization of synapses points toward important principles of cortical organization that relate to current topics in computational neuroscience and machine learning. The open distribution of our data, analyses, and tools enable greater realism in constraining network and synapse models.

Introduction

The study of cortical connectivity in mammalian model systems established foundational circuit diagrams among neurons classified by their morphology and electrophysiology (1–3). Refinement of cell classes by their long-range projections and genetic markers facilitated more detailed microcircuit representations in rodent (4–8). In contrast, studies of human

cortical connectivity (9–14) have been more limited but offer the opportunity to identify features that may contribute to our unique cognitive abilities. Although our knowledge of cell types and circuits in rodents and humans has advanced, a complete description of the connectivity and synaptic properties among cell subclasses in each cortical layer is still lacking (15).

Cortical synapses are dynamic, varying their response strength in ways that are highly stochastic and also modulated by the prior history of activity. The dynamical properties are influenced by both the presynaptic and postsynaptic cell types (16–20) and endow neuronal networks with essential sources of computational diversity (21, 22). As models in neuroscience push toward greater biological realism there is a need for large-scale datasets with a deep description of synaptic dynamics among a diversity of cell types. Likewise, the incorporation of biologically-inspired sources of computational diversity has shown promise in advancing machine learning techniques (23). To meet the needs of the theoretical and experimental research communities, these large datasets need to be open and accessible.

Results

Synaptic Physiology Pipeline

We performed 1,931 experiments (Fig 1A) in acute brain slices targeting intralaminar connections in Layer 2 (L2) to L6 of adult mouse (mean age 46.0 ± 4.6 days) primary visual cortex (VISp; 1,715 experiments) and human fronto-temporal cortex from neurosurgical excised tissue (216 experiments). We utilized transgenic mice that express unique reporters in two subclasses (24) (Table S1). Six excitatory subclasses were layer or projection-class specific (Nr5a1 and Rorb, L4; Sim1 or mscRE4-FlpO AAV, L5 ET; Tlx3, L5 IT; Ntsr1, L6 CT) while three inhibitory subclasses (Pvalb, Sst, Vip) were assessed in all targeted layers (Fig 1A). We probed 23,620 potential connections (mouse: 20,949; human: 2,671) of which 1,731 were connected by chemical synapses, giving an overall connectivity rate of 7.3% (mouse: 1,526 (7.3%); human: 205 (7.7%)).

Details of the experiments are described in Fig. 1B/C and in the Methods. In each experiment, up to eight neurons were selected for simultaneous whole-cell patch-clamp recording primarily in current-clamp, with a subset of stimuli administered in voltage-clamp (Fig 1B). Stimuli were elicited in each patched neuron, in turn, while all others were recorded for evidence of a postsynaptic response. Dynamics (short-term plasticity and variability) of individual connections were assessed from stimulus trains at frequencies ranging from 10 – 200 Hz (Fig 1B). Cells were stimulated with long current pulses to characterize their intrinsic physiology and later stained with biocytin to characterize their morphology (Fig 1C).

Intralaminar connectivity in mouse VISp

Distance dependence of connectivity—The likelihood that two neurons are connected decreases with increasing intersomatic distance (25–27). We probed connectivity among cells up to ~200 μm apart (Fig 2A), but could not ensure that intersomatic distances were sampled equally across different connection elements (specific pre-post combinations). To

make reliable comparisons, we modeled the spatial profile of connectivity versus lateral somatic distance with a Gaussian (25) and estimated the peak (p_{max}) and lateral spread (sigma: σ) of connection probability using maximum likelihood estimation (see Methods, Fig S1B). This analysis provided an estimate of the spatial profile of connectivity while being relatively robust to differences in the sampled intersomatic distribution. We initially classified cell pairs among the four combinations of excitatory and inhibitory cell class (E→E, E→I, I→E, I→I). These data were well fit by the Gaussian model (Fig 2A, solid red line) and indicated low peak connectivity among excitatory cells (5%) with moderate connectivity rates among inhibitory cells (12%) and across E-I cell classes (E→I 12%, I→E 15%). In a tracing study of primary visual cortex L2/3, E→E connections had a wider lateral extent compared to I→E (28). We additionally found that E→E and I→I connections have a similar spatial extent that is larger than both E→I and I→E connections.

An overabundance of bidirectional connections relative to unidirectional connections can be evidence for connectivity rules that promote the formation of bidirectional connections (29). A simpler explanation, however, is that bidirectionality is not specifically promoted in cortex, but rather an artifact of merging connectivity results across cell types (30). We quantified the ratio of connected pairs with and without bidirectional connections and observed that reciprocal connections were 3 to 5 times more common than expected for a randomly connected network (red line) among class-level connections (Fig 2A, bottom row).

Connection probability measurement; slicing artifacts and detection limits: In the *in vitro* slice preparation, some connections may be severed, reducing the measured rate of connectivity (25, 31). To mitigate this bias, we used thick slices (350 μm), targeted cells deep in the slice (Fig S2B, median cell depth = 74 μm), and focused on local (<200 μm apart), intralaminar connections. By modeling the effects of cell depth and axon length on connection probability, we estimated the size of this bias and adjusted our p_{max} measurements accordingly. This yielded an ~3–6% increase in p_{max} when accounting for severed axons (Fig S2A, D) and an ~2–20% increase in p_{max} when accounting for depth of the targeted cells from the slice surface (Fig S2B, D).

Detecting a connection in electrophysiological recordings is influenced by the background electrical noise, which may obscure synaptic responses in the postsynaptic cell. The effect of noise on detection is reduced by averaging the responses to multiple presynaptic action potentials. Over the course of a typical experiment, most cells were stimulated to evoke hundreds of action potentials; however, this number varied significantly from cell to cell (485 [192, 623] action potentials; median [IQR]). To account for the opposing effects of noise and averaging, we quantified the ‘detection power’ (analogous to signal-to-noise ratio; see Methods) for each pair of cells that were probed for connectivity. We observed a range of detection powers across pairs and this data was used to model the effect of detection power on connectivity. A model of the relationship between detection power and connection probability resulted in a 45% increase in estimated p_{max} for excitatory connections and up to 90% increase for inhibitory connections (Fig S2D, E), suggesting that the observed connectivity rate is affected more by detection power than by slicing artifacts. Detection power is seldom reported and may explain cases where the observed connectivity *in vitro* is higher than *in vivo* for the same brain area and connections (32, 33).

We extended our model of connection probability on intersomatic distance (Fig 2A, solid line) to include the effects of slicing and response detection outlined above (see Methods). The model-adjusted connectivity rate resulted in a 1–2 fold increase in estimated p_{max} at the cell class level (Fig 2A dashed line). To confirm these results, we implemented a similar connectivity adjustment by filtering the data for axon lengths, pair depths, and detection power values above their respective median (Fig 2A, dotted line) where the impact on connection probability is reduced (Fig S2A–C). This yielded a comparable increase in estimated p_{max} (Fig 2A dotted vs dashed line) and as such we used the model to adjust peak connectivity estimates at the subclass level where filtering would induce under-sampling. Inhibitory connections received a higher detection power adjustment than excitatory connections. Adjustments for presynaptic axon length and pair depth were relatively uniform across subclasses. (Fig S2E).

Connectivity among cell subclasses—The intralaminar connectivity among mouse VISp subclasses is summarized in Fig 2B (Fig S1A). We found that intralaminar connection probability varies by layer (Fig 2B and C), long-range projection target (Fig 2D), and cell subclass (Fig 2 E, F). Connectivity in superficial layers was overall higher than deep layers. For example, the pyramidal to Pvalb connection in L2/3 (p_{max}=0.79 [0.57, 0.99] 95% CI) compared to L5 (IT p_{max}=0.22 [0.12, 0.35]; χ^2 p=7.2e-54) (Fig 2C, Fig S1A). Recurrent connections between excitatory and Vip cells were common in L2/3 (E→Vip 0.38 [0.21, 0.60]; Vip→E 0.11 [0.03, 0.26]) but rare or absent in deeper layers (Fisher p=6e-4; Fig S1A).

Within L5 we found several differences between two excitatory projection classes, intratelencephalic (IT, labeled by Tlx3) and extratelencephalic (ET, labeled by Sim1 and mscRE4). ET cells overall have more input from local sources relative to IT cells. ET cells have higher recurrent connectivity (χ^2 p=3.17e-6; Fig 2D) as well as receive unidirectional input from IT cells, consistent with previous results (34). Sst cells also innervate ET cells at a higher rate than IT cells (χ^2 p=3.18e-5; Fig 2E–F); a similar connectivity pattern was observed in rat frontal cortex (35).

Sst is thought to avoid connecting with itself (4, 36, 37), however, we observed connections between Sst neurons in every layer (Fig 2B). The Sst-IRES-Cre driver can sparsely label fast-spiking interneurons that also express Pvalb (38). UMAP projection of intrinsic properties from inhibitory cre-types showed that slightly less than half of the recurrent Sst connections had both the pre- and postsynaptic cell in a cluster that was spatially distinct from Pvalb cells, suggesting that these connections came from cells that were intrinsically Sst-like (Fig S3A). We confirmed that, in at least one case, both cells in the pair had axons extending into L1 and sparsely spiny dendrites, consistent with Martinotti neurons (Fig S3B). We performed experiments utilizing the Patch-seq method (39) and further confirmed that cells which transcriptionally mapped to the Sst subclass do form connections with each other (5 connections found out of 66 probed, Fig S3C).

Electrical connections—In addition to chemical synaptic transmission among cell subclasses, electrical connections formed by gap junctions were also found between inhibitory subclasses (Fig S4A). The likelihood of electrical connectivity as a function

of lateral intersomatic distance could be approximated by a Gaussian but with a narrower profile, σ = 74 μm (Fig S4B), compared to chemical connections between inhibitory cells (σ = 127 μm, Fig 2A; p<0.001, Fig S4B). This is consistent with previous reports of electrical connections between nearby Pvalb cells which showed that the average distance between electrically coupled cells was short, 40–80 μm (40, 41). Pvalb cells showed the highest rate of electrical connections (76/922, ~8.2%), while those among Vip cells were the most rare (15/908, 1.6%; χ^2 p=1.8e-10), in contrast to a previous report of Vip electrical connections which were more prevalent (7). A majority of electrical connections were found between like subclasses (164/170, 96%) and were bidirectional (148/170, 87%). The distance of the gap junction from the soma coupled with the potential for some rectification of electrical connections (42) could account for the few cases where reciprocal electrical connections were not observed. The coupling coefficient of electrically coupled pairs was comparable across subclass (Fig S4C) largely due to the lower input resistance of Pvalb cells (Fig S4D). Estimating junctional conductance revealed stronger electrical connections between Pvalb cells (0.38 [0.20, 0.61] nS, median [IQR]) than either Sst (0.23 [0.19, 0.36] nS; MW p=0.02) or Vip (0.07 [0.03, 0.19] nS; MW p=5e-4) (Fig S4C).

Synaptic strength and kinetics

In addition to connectivity, synaptic properties such as strength, latency, and kinetics (rise time and decay tau) determine the impact of a connection on the postsynaptic neuron and, ultimately, on cortical processing. Although these properties have been described previously for some cortical connections(4, 27, 43–46), measuring them systematically across many cell types enabled us to make direct comparisons.

At the class level, inhibitory connections showed short latencies (median=1.07 ms), slow kinetics, and relatively strong PSPs. These trends were largely driven by the subclass of the presynaptic cell and Pvalb in particular. Pvalb connections were extremely fast, with sub-millisecond latencies (Fig 3A) highlighted by Pvalb→L6 excitatory connections (0.94 [0.86, 0.99] ms, median [IQR]). Pvalb cells also elicited large resting state IPSP amplitudes regardless of postsynaptic cell subclass. Presynaptic Sst cells stood out for having some of the slowest kinetics, independent of postsynaptic target (see Sst→Vip rise time: 7.02 [5.65, 9.75] ms, decay: 50.81 [26.97, 142.41] ms; Sst→L5 IT rise time: 7.46 [5.51, 9.92] ms, decay: 58.59 [27.76, 166.83] ms).

In contrast to inhibitory connections, excitatory connections generally had a long latency (median=1.49 ms; KS compared to inhibitory p=1.4e-34), fast kinetics, and weak PSPs, all of which related more to the identity of the postsynaptic cell. Excitatory→Inhibitory connections displayed faster rise times than recurrent excitatory connections (E→I 2.75 ms, E→E 3.88 ms, KS p=2.97e-12, Fig 3B). Recurrent excitatory connections showed some of the smallest amplitudes in the resting state (eg. L5 ET→L5 ET, 0.27 [0.13, 0.49] mV) whereas E→I connections were stronger (Fig 3D, E) and generated the single biggest PSP (9.51 mV, L2/3 Pyr→L2/3 Sst). E→I connection properties can be further refined by postsynaptic cell subclass. Connections with postsynaptic Pvalb cells had faster kinetics (see L4 Pyr→Pvalb, Fig 3; rise time: 1.45 [1.28, 1.94] ms, decay tau: 6.92 [5.4, 8.36] ms) than postsynaptic Sst cells (see L2/3 Pyr→Sst, Fig 3; rise time: 3.91 [2.69, 4.79]

ms, decay tau: 19.41 [14.88, 28.48] ms). A dichotomy between Pvalb and Sst was also apparent in the resting state amplitude with larger EPSPs to Pvalb cells (0.41 [0.22, 0.79] mV) than Sst cells (0.08 [0.05, 0.25] mV); however, the strongest excitatory connections were onto Vip cells found predominantly in superficial layers (L2/3 pyr→Vip 0.45 [0.26, 0.84] mV). Although resting state excitation was weakest on to Sst cells, resting state PSP amplitude is an underestimate of the potential impact on the postsynaptic cell particularly for connections that strongly facilitate. When we compared the 90th percentile amplitude (Fig 3E), which measures near-maximal strength, E→Sst connections were comparatively stronger, and even surpass E→Pvalb amplitudes in some cases (see L2/3 Pyr→Sst vs L4 Pyr→Pvalb). Facilitation onto inhibitory cells further contributes to the longer tails of 90th percentile amplitudes and the rightward shift of E→I (0.73 mV) amplitudes compared to E→E (0.34 mV, KS p=1.53e-14; Fig 3E, histograms).

A recent survey of cortical connectivity found that connection strength positively correlated with connection probability (6). This result suggests an interesting principle of connectivity, but may also result from the reduced detectability of weaker connections. When we adjusted for detection power, connection probability was independent of connection strength for both excitatory (weighted Huber regression $r^2 = -0.1$, $p = 0.8$) and inhibitory ($r^2 = 0.2$, $p = 0.2$) connections.

Synaptic dynamics

The strength and kinetic properties described above characterize the synapse in response to a single presynaptic spike; however, synapses are highly dynamic. PSP amplitude evolves in predictable ways over the course of milliseconds to seconds due to short-term plasticity (STP), while also being highly stochastic from one response to the next, quantified by the coefficient of variance. Overall, synaptic dynamics followed a similar pattern to synaptic strength, wherein excitatory connections were most strongly differentiated by the postsynaptic subclass and inhibitory connections were differentiated by the presynaptic subclass. The STP of a synapse may result in a transient increase (facilitation), decrease (depression), or no change (pseudo-linear) in PSP amplitude over the course of a stimulus train as is seen in our data (Fig 4A) and has been described previously (16, 20, 47–49). The time course of recovery from STP is an equally important property of synapses, yet one that is not well described. The variable delays we imposed between the induction and recovery pulses (Fig 1B, *Multipatch Experiment*) of our 50 Hz stimulus showed that at our earliest time point (125 ms), connections were still in their STP induced state, but that by four seconds they were largely recovered.

Excitatory dynamics were strongly aligned with postsynaptic cell class (49), and further refined by layer in the case of excitatory targets and by subclass of inhibitory targets. Recurrent excitatory connections were largely depressing (Fig 4B, E L5ET→L5ET) and showed increasing depression with stimulus frequency (Fig 4F). Recurrent excitatory connections occupy a range of recovery and variability profiles that vary with layer. Superficial layers (eg. L2/3→L2/3) tended to recover more quickly (Fig 4C) and showed a higher degree of variability (Fig 4D). E→I dynamics depend on the subclass of the postsynaptic target. Excitatory to Sst cells were strongly facilitating, consistent with

previous reports (48, 50). E→Sst connections were also highly variable in the resting state, likely owing to a high initial failure rate (Fig 4A, middle, pulse 1, Fig 4E); however, strongly facilitating synapses often become more reliable in the induced state (Fig 4A, middle, pulse 8, Fig 4E). Excitatory connections onto Pvalb (Fig 4E, L4 pyr→Pvalb) were largely depressing on average, though a subset of connections in L2/3 showed pseudo-linear STP similar to *in vivo* measurements in somatosensory cortex(45). While these patterns of excitatory dynamics were apparent on average, multiple measurements of synaptic dynamics show high heterogeneity from pair to pair within a connection type (Fig 4E).

Dynamics of inhibitory connections showed patterns more related to the subclass identity of the inhibitory presynaptic cell. Pvalb connections onto other subclasses, both excitatory (Fig 4E, Pvalb→L6 pyr) and inhibitory, were strongly depressing (Fig 4B) and still depressed at our earliest recovery time point (Fig 4C). Depressing Pvalb connections showed high reliability at the beginning of a stimulus train (resting state log variability = −1.01; Fig 4D) and became more variable in their STP induced state (log variability = −0.27, MW p=3.65e-31; eg Fig 4E). Connections from Sst and Vip cells had a mixture of dynamics from facilitation to moderate depression (Fig 4E, Sst→L5 IT). These connections were also faster to recover from STP, particularly Sst connections which tended to over-recover at the shortest interval (Fig 4C).

Synaptic interactions between Sst and Vip were an exception to the trends highlighted above. Whereas most inhibitory connections were depressing, Sst→Vip (7) showed the highest degree of facilitation in our dataset (0.28 [0.0, 0.44]). The reciprocal Vip→Sst connection was weakly facilitating, as were recurrent Vip connections. These three connection types also over-recovered on short time scales (Fig 4C) and took many seconds to fully recover (Fig 4F). Given the facilitating nature of these connections it is interesting to note that they had only a moderate degree of variance (resting state log variability = −0.03; Fig 4D) compared to other facilitating connections such as E→Sst (resting state log variability = 1.66; MW p=−3.0e-8).

Human intralaminar connectivity

As a complement to the mouse visual cortex, our dataset includes synaptic physiology from human temporal cortex. Although our sampling of human connections covered all cortical layers, our analysis focused on the supragranular layers, which are expanded in anthropoid primate cortex (51). Deep L3 cells have distinct electrophysiology, morphology, and gene expression (including genes involved in connectivity and synaptic signaling) and many of these properties vary continuously with depth between L2 and L3b (52). Dense sampling of L2/3 allowed us to define L2, L3a, and L3b pyramidal subclasses and demonstrate that these principles of cellular diversity have correlates in synaptic physiology. These subclasses showed distinct synaptic properties including unique polysynaptic connections from L2 cells and STP that closely follows the continuous variability between L2/3 subclasses.

Distance dependence of connections was modeled and adjusted as with mouse connections, but without distinguishing connections by cell class (most connections were recurrent excitatory). Connection probability was estimated to fall off with distance at a lateral spread (σ) of 130 μm (Gaussian model fit, Fig S5A), slightly larger than the comparable value

in mouse (125 μm for within-class connections), reflecting that while cortical expansion is accompanied by the scaling of neuronal morphology, much of this scaling is axial rather than lateral. Examining the connectivity between subclasses (Fig 5A), we tested for signatures of functional segregation within supragranular layers, finding a strong bias for recurrent over cross-connections between L3a and L3b (Fisher p=5.6e-3) and a bias for connections from L2 to L3a over L3b (Fisher p=3.4e-3).

Recurrent connectivity within human L4 (p_{max}=0.01 [0.0, 0.04] 95% CI, 1/145) was significantly lower than observed in the mouse (p_{max}=0.22 [0.16, 0.28], 44/452; Fisher p=1.4e-4). This contrast could be related to age (37), species, or brain area. Furthermore, we observed other connections involving L4 pyramidal cells (e.g. I→E and E→I), suggesting that low excitatory recurrence was not a technical limitation of our dataset, but rather reveals a unique property of the human L4 circuit.

Human synaptic properties

The strength, kinetics, and STP properties of the human connections showed moderate differences across layers and large differences by cell class, largely resembling observations in mouse (Fig 5B). Recurrent excitatory connections in human cortex (E→E) have longer latency than those with a pre- or postsynaptic inhibitory cell (E→E median 1.73 ms vs. I→E 1.04 ms, KS test p=2.2e-5; E→I 1.34 ms, p=2.4e-3), and PSP rise times were faster for E→I than E→E connections (2.42 ms vs. 4.10 ms, p=2.0e-8), but slower for I→E connections (5.72 ms; p=5.3e-3, 4.9e-6 vs. E→E, E→I). We observe some differences between L2 and L3, including presynaptic L3 cells forming more depressing connections than L2 cells (STP ratios −0.39 vs.−0.15, p=9.2e-3). E→I connections were uniformly depressing, consistent with the identification of those inhibitory cells as fast-spiking Pvalb cells.

In certain properties, we did observe contrasts between human and mouse connections. The amplitudes of L2/3 excitatory PSPs were generally larger in human. For E→E connections the contrast was stronger for 90th percentile response (0.51 mV vs. 0.30 mV, p=0.019), while for E→I connections the contrast was stronger for resting state response (0.91 mV vs. 0.26 mV, p=2.2e-3), due to significantly more depressing E→I connections in human (−0.51 vs 0.05, p=7.1e-6). We also observed faster recovery from STP in human than mouse excitatory connections, with most fully recovered at 500 ms (Fig 5C). This contrast has been previously noted in recurrent L2/3 excitatory connections (12); our observations suggest that it holds for L2/3 E→I connections also.

Human polysynaptic events—We found short-latency (~3 ms) inhibition (Fig 5D) following stimulation of excitatory cells, indicating activation of polysynaptic connections. Plotting latency versus PSP amplitude of human connections (Fig 5D) revealed a clear boundary where responses with a latency of 3 ms or greater, evoked from a confirmed pyramidal cell, were almost exclusively inhibitory (median latency of IPSPs: 4.19 [3.79, 4.81] ms), compared to monosynaptic EPSPs which had a latency less than 3 ms (median EPSP latency: 1.71 [1.44, 2.22] ms). This potential disynaptic inhibition (dIPSPs) originated in L2 and projected to other L2 (n=8) or L3 (n=11) pyramidal cells, with just one ascending polysynaptic response originating in L3. This directionality was consistent with

the directionality of monosynaptic excitation across layers 2 and 3 as well as supported by higher connection rates from L2 pyramidal cells to inhibitory cells.

Variation with depth in human layers 2 and 3—Another property of supragranular neurons observed in human, but not in mouse, is strong depth-driven variability of intrinsic electrophysiological properties (52, 53). Visualizing the electrophysiology feature space by a UMAP projection of 27 electrophysiology features (Methods), we found that L4-type cells (high input resistance) are situated around the perimeter, indicating distinct properties from L2/3-type cells (Fig 5E). For the L2/3-type cells, projecting a normalized layer depth coordinate (relative to the L2+L3 thickness) onto this space showed a mostly smooth gradient of electrophysiological properties with layer depth, also verified by direct examination of depth correlations with sag and AP upstroke/downstroke ratio (p=7.0e-6, 3.3e-5) (Fig 5F). This correlation was not found in mouse L2/3 cells (p>0.06 for both).

STP metrics revealed a similar linear variation with layer depth in connections from L2/3 pyramidal cells across both E→E (n=86 human, n=15 mouse) and E→I (n=20 human, n=72 mouse) connections. The paired-pulse STP showed a strong linear relationship with depth in the human data (p=5.4e-4), varying from weak facilitation for the most superficial cells (0.02 ± 0.03, mean±SEM) to depression for the deepest (−0.32 ± 0.09). A strong correlation was also found with the action potential upstroke/downstroke ratio of the presynaptic cell only (p=1.2e-4 vs p>0.3 for postsynaptic) (Fig 5G). No corresponding trends were found in the mouse data (p>0.2 for all regressions). Although lower sampling of L2/3 pyramidal cells may contribute, regression coefficients for STP against upstroke/downstroke ratio show a strong contrast (human −0.16 [−0.24, −0.08] CI; mouse 0.05 [−0.03, 0.13]), suggesting that there are real differences between these datasets in the factors contributing to STP variability, whether explained by species, brain area, or other factors.

Modeling short term plasticity of mouse and human connections

The STP metrics introduced above were chosen for their ease of interpretation, but have several drawbacks: they are sensitive to noise, they require successfully repeated stimuli that are not available for all connections, and they are difficult to use in a biophysical modeling context. Ideally, we would like a description that incorporates all of the data available for each connection and can predict synapse behavior in response to any arbitrary stimulus. We developed a generative model of stochastic vesicle release and STP with several adjustable parameters (see Methods) and asked which combinations of parameters could best explain the responses recorded for each connection. In this way, we captured and described more of the dynamic behavior of each connection with a small number of parameters. Our approach is similar to other recently developed models (54, 55) in that it does not depend on any particular stimulus structure (aside from having a diversity of interspike intervals). Accordingly, the model results for each connection make use of all presynaptic spikes and are robust to spike failures and early experiment termination.

Model performance was evaluated by using the maximum likelihood parameter set for each connection to simulate experimental data. This simulated data was then used to generate the same STP metrics that were previously collected from synaptic data. Both resting state

PSP amplitude and 90th percentile amplitude were almost perfectly correlated between recorded and simulated data (Fig S6A,B), indicating that the model does exceptionally well at capturing synaptic strength. STP and variability (Fig S6C–F) were also strongly correlated, but with more scatter relative to strength metrics. STP measured from the second pulse in 50 Hz trains was only half as large as measured in synaptic responses, indicating that the model as parameterized was not able to fully capture STP on this timescale. Release probability was more highly correlated with variance than number of release sites, suggesting that synapses may control variability primarily through their release probability.

Most discussions of short term depression in the cortical literature begin with the assumption that depression is caused by the depletion of vesicles from the readily-releasable pool. However, recent evidence suggests that calcium channel inactivation may be a more prominent mechanism in cortical depression (56). We ran the model on two separate parameter spaces--one that uses vesicle depletion, and another that uses a release-independent depression mechanism. In most cases, the model maximum likelihood value was found in the release-independent parameter space (Fig S7E, left). Release-dependent depression mechanisms should result in negative correlation between consecutive PSP amplitudes; however, we found little evidence for such negative correlations in our mouse data. Likewise, we found little relationship between paired correlation values and the model preference for release-dependent mechanisms (Fig S7E, right). These results are consistent with the proposal that cortical synapses in mouse employ release-independent depression mechanisms, and that vesicle depletion plays a relatively minor role in depression. In comparison, our data from human connections had a modest preference for negative correlation between paired event amplitudes.

Organization in mouse and human synaptic dynamics

With a large dataset describing synaptic properties of connections it becomes possible to ask what patterns emerge from the data. What synaptic features correlate with one another, and do connections naturally split into clusters based on these features, or do they form a continuum? What aspects of the synaptic feature-space are driven by presynaptic versus postsynaptic cell type? Excitatory connections onto Pvalb and Sst cells have distinctly different dynamics, suggesting a general rule that excitatory dynamics depend primarily on the postsynaptic cell type (16, 57). In contrast, inhibitory dynamics depend mainly on the presynaptic type, particularly when comparing Pvalb to Sst (48, 58). Although our data often followed these rules, we also found exceptions and suggest some refinements.

We used the stochastic release model described above to characterize 1196 connections (1035 mouse, 161 human). Although it would have been possible to use the maximum likelihood parameter set to describe each connection, parameters derived in this way are sensitive to experimental noise (59). Thus we generated a more robust representation of synaptic behavior by exhaustively searching a large parameter space for each connection, then used sparse PCA followed by UMAP dimensionality reduction to summarize these results (Fig 6). This analysis groups connections based on the similarity of their model results; therefore, it has access to any synaptic strength and dynamical properties that the model could capture, but does not have access to information about kinetics, cell subclass,

or other cell properties. Connections in this analysis formed clear excitatory and inhibitory clusters (Fig 6A), with a continuum of synaptic properties within each cluster. Perhaps the most prominent feature of this organization was that excitatory connections were strongly differentiated by the postsynaptic E/I class (66% classifier accuracy gain relative to shuffled; see Methods), whereas inhibitory connection properties were mostly independent of postsynaptic cell class (7% gain).

Several synaptic properties were found to have a clear relationship to the UMAP organization (Fig 6B). Which of these properties best explain the separation of excitatory synapses by postsynaptic class? We generated a list of features from the maximum likelihood models and ranked these by the strength of their relationship to cell subclasses (see Methods). When distinguishing between E→E and E→I connections, features that describe quantal release and synapse variance made up 8 out of the top 10 features (Table S2). In contrast, STP parameters had relatively low importance in this classification, and the effect of synaptic strength was negligible. This relationship was also apparent when classifying excitatory connections between excitatory, Pvalb, Sst, and Vip postsynaptic subclasses (48% gain; Fig 6B). Again, this relationship appears to be driven by quantal release parameters and variability metrics, whereas STP metrics were somewhat less important. Only minor relationships were found between excitatory synapse properties and postsynaptic excitatory subclasses (13% gain; Fig 6C) or inhibitory synapse properties and postsynaptic subclasses (E and inhibitory subclasses: 14% gain; excitatory subclasses: 5% gain; Fig 6B). To simplify, excitatory synapses have low variability when the postsynaptic cell is excitatory, high variability when the postsynaptic cell is inhibitory, and highest variability onto Sst cells.

Inhibitory synapses, in contrast, did not follow this pattern. Instead, inhibitory synapse properties were more predictive of the presynaptic subclass (41% gain). The parameters that most contributed to this relationship include STP, variability, and to a lesser degree synaptic strength. Excitatory synapses were more weakly affected by presynaptic subclass (24% gain), but this relatively small effect appeared to be similarly driven by differences in STP and variability.

Human E→E synapses were strongly differentiated from mouse E→E (43% gain). This was driven by a more diverse set of properties including STP (especially recovery), variability, facilitation time constant, and strength (Table S2, last column).

Discussion

By probing over 20,000 possible connections across 28 mouse lines, we have explored a large fraction of the subclass-specific, intralaminar connectivity in the mouse visual cortex. In addition, we sampled connections in the human cortex using similar methods for comparison. Past surveys near this scale have focused on connectivity and strength of connections; a major advance provided by our study is the depth of characterization and analysis for each connection, in the context of transgenically identified cell subclasses and species.

A proposed standardized model of connectivity

The likelihood that two neurons are locally connected depends on multiple factors such as cell type, cortical region, species, and animal age. A longstanding goal has been to determine the governing principles of local circuit architecture. It is difficult to make direct comparisons among different studies because the observed rate of connectivity depends on several experimental details that are often inadequately reported or controlled for. Ideally, we would like a way to describe connectivity that allows more direct comparison between experiments regardless of their methodological differences. In order to facilitate such comparison between connection subclasses in our own data, we developed a procedure for modeling connection probability as it relates to intersomatic distance, axon truncation, cell depth, and signal detection power. With this model, we can estimate unbiased connection probabilities with confidence intervals that should be relatively robust to experimental bias. In principle, this approach is flexible enough to be replicated elsewhere in the field and its adoption would substantially improve our ability to compare and reproduce results across studies.

Conserved and canonical elements in the mouse intralaminar circuit

As many prior studies have investigated the cortical circuit, a picture has emerged describing the relationships between the excitatory and inhibitory subclasses and their functional relevance. The details of this picture vary somewhat between descriptions, but a few key elements appear consistently, especially in the systems and theoretical neuroscience literature (Fig 7A). Pvalb interneurons strongly inhibit nearby pyramidal cells and other Pvalb cells, Sst interneurons broadly inhibit nearby cells but avoid other Sst cells, and Vip cells selectively inhibit Sst cells and receive feedback excitation, forming a disinhibitory circuit (60, 61). We confirmed that each of these motifs is prominent across layers in the intralaminar cortical circuit.

Other circuit elements are equally prominent in our data but are more sparsely acknowledged in the literature. Many recent studies have focused on the importance of the Vip→Sst disinhibitory circuit. In the opposite direction, however, the connection from Sst to Vip has one of the highest connection probabilities, largest IPSP amplitudes, and strongest facilitation in our dataset. Although Sst→Vip connections have been described previously (4, 6, 7), they are often overlooked in consideration of the disinhibitory circuit. The synaptic features we observed suggest an important functional ramification on the opposing Vip→Sst disinhibitory pathway (60, 62, 63).

Sst and Vip cells are often described as lacking recurrent connections (36, 37, 49, 64) despite some evidence to the contrary (6, 65). We confirmed that Sst and Vip do have the expected biases in their connectivity across all layers (Sst cells tend to avoid contacting other Sst cells and Vip cells prefer to contact Sst cells). However, we also found sparse, recurrent connections within both interneuron populations about equal to the recurrent connectivity in excitatory populations. Furthermore, the strength of connections from Sst and Vip did not follow the same preferences, having roughly equal strength when connecting to preferred versus non-preferred subclasses. Given their trans-laminar axon projection

patterns, recurrent connections within these subclasses may be found more commonly across layer boundaries (66).

Laminar variations on the cortical circuit

Previous studies that sampled both L2/3 and L5 noted many similarities between the two layers (4, 6). Although we confirmed a consistent set of connectivity rules describing the intralaminar circuit, we also found variations on these rules that could support different modes of cortical function. Differences in intralaminar circuitry may contribute to laminar differences in receptive field properties (67) or visually mediated behaviors (61).

Layer 2/3 has strong interconnections between pyramidal and inhibitory cells (Fig 7B). In deep layers, these connections are either absent or greatly reduced, and the relative sparsity of Vip cells, in particular, in deep layers should further enhance these differences (68, 69). Direct Vip inhibition of local pyramidal cells further complicates the prevailing view of the Vip→Sst disinhibitory pathway by, for example, allowing the possibility of feedback inhibition from higher cortical regions. Likewise, local excitatory inputs to Vip cells could be a source of feedforward disinhibition in layer 2/3.

Layer 5 excitatory subclasses differ in their visual responses and long range projections, suggesting different functional roles in the circuit (70, 71). Accordingly, we saw differences in the intralaminar connections of L5 ET and IT neurons. ET pyramidal cells were generally more highly connected, receiving more local excitation and inhibition than IT cells. We confirmed a much higher rate of recurrent connections among L5 ET cells compared to IT as well as the observation that connections between these two subclasses were unidirectional from IT→ET (Fig 7C) (34). Layer 5 ET cells also received more frequent inhibition from Sst cells, as previously observed in frontal cortex of rat (35).

Could laminar differences in connectivity indicate cell type divisions within subclasses? Two recent studies investigated the correspondence between morphological, electrophysiological, and transcriptomic (MET) features of inhibitory neurons in primary visual cortex and motor cortex (66, 72). In visual cortex, different MET types had distinct patterns of local axonal innervation and dendritic morphologies (66) suggesting that their connectivity will be different. MET types also exhibited layer localization and thus some of the differences in connectivity we observe as a function of layer may reflect differences in connectivity between different MET types.

Dynamic flexibility in the cortical circuit

Most studies in cortical synaptic physiology describe the circuit in its quiescent state. Ongoing activity *in vivo*, however, can transiently depress or facilitate synapses in a cell type-dependent way. In effect, the cortical circuit is modified from moment to moment based on the recent history of activity, and thus it may be misleading to conceptualize the cortex as a single, static circuit diagram. Although STP is variable across individual synapses, many subclass elements of the cortical circuit had a clear preference for either facilitation or depression (Fig 7D). These patterns suggest an ability to dynamically switch between different network modalities where intralaminar activity shifts from depressing interactions between pyramidal and Pvalb cells at the onset of activity, to facilitating interactions

between pyramidal, Sst, and Vip cells during sustained activity. Ultimately, activity patterns *in vivo* determine the extent of STP in each cell type, and the functional effects have yet to be determined.

Excitatory cells receive weak local excitation compared to inhibitory cells

Our previous study (13) observed low recurrent excitatory connectivity rates in all layers. We now find that recurrent excitatory connections have a set of features that distinguish them from excitatory inputs to inhibitory cells and appear to limit their contribution to excitability. In addition to being sparse, they are relatively weak, they get weaker with activity, and they have slower PSP rise times. Slow PSP rise times limit excitability by raising action potential threshold (73). Slow rise times have been attributed to the PSPs being less synchronous at the multiple synapses that form E-E connections (74). Unlike the relatively high rate of intralaminar connectivity for E-I connections observed in all layers, recurrent excitatory connectivity is generally lower, and nearly absent in human L4 and in CT cells of mouse L6.

Unidirectional disynaptic inhibition in human

We observed disynaptic inhibition in human cortex between confirmed spiny pyramidal cells that is unidirectional, originating in L2 and targeting other L2 or L3 pyramidal cells. We did not see disynaptic inhibition in our mouse recordings, which may be due to the stronger excitation we, and others (9), observe in human connections, particularly onto inhibitory cells. Disynaptic inhibition is often mediated by an interposed Sst cell (75, 76) because they have a low spiking threshold and receive facilitating inputs from excitatory cells. However, the latency of Sst-mediated disynaptic inhibition is often long (> 100 ms) whereas we saw disynaptic IPSPs with a much shorter latency (3 – 6 ms). This suggests the disynaptic inhibition is driven by an intermediate fast-spiking Pvalb cell which has been observed in humans and can be recruited by very large excitatory events (14). The unidirectional nature of this disynaptic inhibition from more superficial to deeper cortex further suggests a preferential routing of information by Pvalb cells in human cortex (14).

Connection types differ in variability

We used a novel model of stochastic vesicle release and STP to estimate parameters that best describe each connection. A few governing principles emerge from this analysis. Cortical connection types could be organized into a two-dimensional feature space, with synaptic strength and variability forming two orthogonal gradients. Excitatory connections are grouped along the variability axis based on their postsynaptic subclass: these connections have lower variability when connecting to excitatory cells, higher variability onto Pvalb cells, and the highest onto Sst cells. In contrast, inhibitory connections partition more naturally based on their presynaptic subclass. This partition again separates connections based on variability, with Pvalb connections having overall lower variability than other inhibitory types. In most cases, variability correlates with STP--the highest variance connections are more likely to be facilitating. The rules derived from these relationships are similar to rules described previously (48, 49, 77). However, we found synaptic variability to be a better predictor of cell subclass than STP or strength, particularly for excitatory connections.

Synaptic variability has been regarded as an undesirable consequence of signaling via metabolically expensive exocytosis. More recently, advances in machine learning that rely on stochasticity have supported the possibility that synaptic variability may offer computational benefits, such as a mechanism for regularization during learning (21). If that is the case, it is further plausible that variability may be modulated by cell type, and that these relationships are crucial features of cortical function. Indeed, our measurements of synaptic variability strongly differentiated cell type in a pattern that is largely, but not entirely, aligned with STP metrics, suggesting the possibility of cell type-specific tuning of variability. More broadly, analysis of our stochastic release model indicates that synaptic strength and variability form the two most significant parameters describing synapse behavior.

Supplementary Material

Refer to Web version on PubMed Central for supplementary material.

Authors

Luke Campagnola[1,*], Stephanie C Seeman[1,*], Thomas Chartrand[1], Lisa Kim[1], Alex Hoggarth[1], Clare Gamlin[1], Shinya Ito[1], Jessica Trinh[1], Pasha Davoudian[1], Cristina Radaelli[1], Mean-Hwan Kim[1], Travis Hage[1], Thomas Braun[2], Lauren Alfiler[1], Julia Andrade[1], Phillip Bohn[1], Rachel Dalley[1], Alex Henry[1], Sara Kebede[1], Alice Mukora[1], David Sandman[1], Grace Williams[1], Rachael Larsen[1], Corinne Teeter[1,†], Tanya L. Daigle[1], Kyla Berry[1,†], Nadia Dotson[1], Rachel Enstrom[1], Melissa Gorham[1], Madie Hupp[1], Samuel Dingman Lee[1], Kiet Ngo[1], Philip R Nicovich[1], Lydia Potekhina[1], Shea Ransford[1], Amanda Gary[1], Jeff Goldy[1], Delissa McMillen[1], Trangthanh Pham[1], Michael Tieu[1], La'Akea Siverts[1], Miranda Walker[1], Colin Farrell[1], Martin Schroedter[1], Cliff Slaughterbeck[1], Charles Cobb[3], Richard Ellenbogen[4], Ryder P Gwinn[5], C. Dirk Keene[6], Andrew L Ko[4,7], Jeffrey G Ojemann[4,7], Daniel L Silbergeld[4], Daniel Carey[1], Tamara Casper[1], Kirsten Crichton[1], Michael Clark[1], Nick Dee[1], Lauren Ellingwood[1], Jessica Gloe[1], Matthew Kroll[1], Josef Sulc[1], Herman Tung[1], Katherine Wadhwani[1], Krissy Brouner[1], Tom Egdorf[1], Michelle Maxwell[1], Medea McGraw[1], Christina Alice Pom[1], Augustin Ruiz[1], Jasmine Bomben[1], David Feng[1], Nika Hejazinia[1], Shu Shi[1], Aaron Szafer[1], Wayne Wakeman[1], John Phillips[1], Amy Bernard[1], Luke Esposito[1], Florence D D'Orazi[1], Susan Sunkin[1], Kimberly Smith[1], Bosiljka Tasic[1], Anton Arkhipov[1], Staci Sorensen[1], Ed Lein[1], Christof Koch[1], Gabe Murphy[1], Hongkui Zeng[1], Tim Jarsky[1,✉]

Affiliations

[1.]Allen Institute for Brain Science, Seattle, WA, USA

[2.]Byte Physics (), Berlin, Germany

[3.]The Ben and Catherine Ivy Center for Advanced Brain Tumor Treatment, Swedish Neuroscience Institute, Seattle, WA, USA

[4.]Department of Neurological Surgery, University of Washington, Seattle, WA, USA

[5.]Epilepsy Surgery and Functional Neurosurgery, Swedish Neuroscience Institute, Seattle, WA, USA

[6.]Department of Pathology, University of Washington, Seattle, WA, USA

[7.]Regional Epilepsy Center at Harborview Medical Center, Seattle, WA, USA

Acknowledgments:

The authors wish to acknowledge the founder of the Allen Institute, Paul G. Allen, for his vision, encouragement and support.

Funding:

R01DA036909 (BT)

RF1MH121274 (BT)

U19MH114830 (HZ)

U01MH114812 (EL, TC)

Data and materials availability:

All data and tools are available from our web portal at https://portal.brain-map.org/explore/connectivity/synaptic-physiology.

References and Notes

1. Thomson AM, Bannister AP, Interlaminar Connections in the Neocortex. Cereb Cortex. 13, 5–14 (2003). [PubMed: 12466210]
2. Markram H, Toledo-Rodriguez M, Wang Y, Gupta A, Silberberg G, Wu C, Interneurons of the neocortical inhibitory system. Nat Rev Neurosci. 5, 793–807 (2004). [PubMed: 15378039]
3. Douglas RJ, Martin KAC, Neuronal circuits of the neocortex. Neuroscience. 27, 419–451 (2004).
4. Pfeffer CK, Xue M, He M, Huang ZJ, Scanziani M, Inhibition of inhibition in visual cortex: the logic of connections between molecularly distinct interneurons. Nature Neuroscience. 16, 1068–1076 (2013). [PubMed: 23817549]
5. Harris KD, Shepherd GMG, The neocortical circuit: themes and variations. Nat Neurosci. 18, 170–181 (2015). [PubMed: 25622573]
6. Jiang X et al. , Principles of connectivity among morphologically defined cell types in adult neocortex. Science. 350, aac9462 (2015).
7. Karnani MM et al. , Cooperative Subnetworks of Molecularly Similar Interneurons in Mouse Neocortex. Neuron. 90, 86–100 (2016). [PubMed: 27021171]
8. Tremblay R, Lee S, Rudy B, GABAergic Interneurons in the Neocortex: From Cellular Properties to Circuits. Neuron. 91, 260–292 (2016). [PubMed: 27477017]
9. Molnár G et al. , Complex Events Initiated by Individual Spikes in the Human Cerebral Cortex. Plos Biol. 6, e222 (2008). [PubMed: 18767905]
10. Molnár G et al. , Human pyramidal to interneuron synapses are mediated by multi-vesicular release and multiple docked vesicles. Elife. 5, e18167 (2016). [PubMed: 27536876]
11. Peng Y, Mittermaier FX, Planert H, Schneider UC, Alle H, Geiger JRP, High-throughput microcircuit analysis of individual human brains through next-generation multineuron patch-clamp. Elife. 8, e48178 (2019). [PubMed: 31742558]
12. Testa-Silva G et al. , High Bandwidth Synaptic Communication and Frequency Tracking in Human Neocortex. Plos Biol. 12, e1002007 (2014). [PubMed: 25422947]

13. Seeman SC et al. , Sparse recurrent excitatory connectivity in the microcircuit of the adult mouse and human cortex. Elife. 7, e37349 (2018). [PubMed: 30256194]
14. Szegedi V et al., Eneuro, in press, doi:10.1523/eneuro.0260-17.2017.
15. Billeh YN et al. , Systematic Integration of Structural and Functional Data into Multi-scale Models of Mouse Primary Visual Cortex. Neuron (2020), doi:10.1016/j.neuron.2020.01.040.
16. Reyes A, Lujan R, Rozov A, Burnashev N, Somogyi P, Sakmann B, Target-cell-specific facilitation and depression in neocortical circuits. Nat Neurosci. 1, 279–285 (1998). [PubMed: 10195160]
17. Blackman AV, Abrahamsson T, Costa RP, Lalanne T, Sjöström PJ, Target-cell-specific short-term plasticity in local circuits. Frontiers Synaptic Neurosci. 5, 11 (2013).
18. Larsen RS, Sjöström PJ, Synapse-type-specific plasticity in local circuits. Curr Opin Neurobiol. 35, 127–135 (2015). [PubMed: 26310110]
19. Lefort S, Petersen CCH, Layer-Dependent Short-Term Synaptic Plasticity Between Excitatory Neurons in the C2 Barrel Column of Mouse Primary Somatosensory Cortex. Cereb Cortex. 27, 3869–3878 (2017). [PubMed: 28444185]
20. Markram H et al. , Reconstruction and Simulation of Neocortical Microcircuitry. Cell. 163, 456–492 (2015). [PubMed: 26451489]
21. Llera-Montero M, Sacramento J, Costa RP, Computational roles of plastic probabilistic synapses. Curr Opin Neurobiol. 54, 90–97 (2019). [PubMed: 30308457]
22. Abbott LF, Regehr WG, Synaptic computation. Nature. 431, 796–803 (2004). [PubMed: 15483601]
23. Burnham D, Shea-Brown E, Mihalas S, Learning to Predict in Networks with Heterogeneous and Dynamic Synapses. bioRxiv (2021), doi:10.1101/2021.05.18.444107.
24. Daigle TL et al. , A Suite of Transgenic Driver and Reporter Mouse Lines with Enhanced Brain-Cell-Type Targeting and Functionality. Cell. 174, 465–480.e22 (2018). [PubMed: 30007418]
25. Levy RB, Reyes AD, Spatial Profile of Excitatory and Inhibitory Synaptic Connectivity in Mouse Primary Auditory Cortex. J Neurosci. 32, 5609–5619 (2012). [PubMed: 22514322]
26. Perin R, Berger TK, Markram H, A synaptic organizing principle for cortical neuronal groups. Proc National Acad Sci. 108, 5419–5424 (2011).
27. Holmgren C, Harkany T, Svennenfors B, Zilberter Y, Pyramidal cell communication within local networks in layer 2/3 of rat neocortex. J Physiology. 551, 139–153 (2003).
28. Rossi LF, Harris KD, Carandini M, Spatial connectivity matches direction selectivity in visual cortex. Nature. 588, 648–652 (2020). [PubMed: 33177719]
29. Song S, Sjöström PJ, Reigl M, Nelson S, Chklovskii DB, Highly Nonrandom Features of Synaptic Connectivity in Local Cortical Circuits. Plos Biol. 3, e68 (2005). [PubMed: 15737062]
30. Hoffmann FZ, Triesch J, Nonrandom network connectivity comes in pairs. Netw Neurosci. 1, 31–41 (2017). [PubMed: 29601066]
31. Stepanyants A, Martinez LM, Ferecskó AS, Kisvárday ZF, The fractions of short- and long-range connections in the visual cortex. Proc National Acad Sci. 106, 3555–3560 (2009).
32. Lefort S, Tomm C, Sarria J-C, Petersen C, The Excitatory Neuronal Network of the C2 Barrel Column in Mouse Primary Somatosensory Cortex. Neuron. 61, 301–316 (2009). [PubMed: 19186171]
33. Jouhanneau J-S, Kremkow J, Dorrn AL, Poulet J, In Vivo Monosynaptic Excitatory Transmission between Layer 2 Cortical Pyramidal Neurons. Cell Reports. 13, 2098–2106 (2015). [PubMed: 26670044]
34. Brown SP, Hestrin S, Intracortical circuits of pyramidal neurons reflect their long-range axonal targets. Nature. 457, 1133–1136 (2009). [PubMed: 19151698]
35. Morishima M, Kobayashi K, Kato S, Kobayashi K, Kawaguchi Y, Segregated Excitatory–Inhibitory Recurrent Subnetworks in Layer 5 of the Rat Frontal Cortex. Cereb Cortex. 27, 5846–5857 (2017). [PubMed: 29045559]
36. Naka A et al. , Complementary networks of cortical somatostatin interneurons enforce layer specific control. Elife. 8, e43696 (2019). [PubMed: 30883329]
37. Scala F et al. , Layer 4 of mouse neocortex differs in cell types and circuit organization between sensory areas. Nat Commun. 10, 4174 (2019). [PubMed: 31519874]

38. Hu H, Cavendish JZ, Agmon A, Not all that glitters is gold: off-target recombination in the somatostatin-IRES-Cre mouse line labels a subset of fast-spiking interneurons. Front Neural Circuit. 7, 195 (2013).
39. Lee BR et al. , Scaled, high fidelity electrophysiological, morphological, and transcriptomic cell characterization. Elife. 10, e65482 (2021). [PubMed: 34387544]
40. Galarreta M, Hestrin S, A network of fast-spiking cells in the neocortex connected by electrical synapses. Nature. 402, 72–75 (1999). [PubMed: 10573418]
41. Galarreta M, Hestrin S, Electrical and chemical synapses among parvalbumin fast-spiking GABAergic interneurons in adult mouse neocortex. Proc National Acad Sci. 99, 12438–12443 (2002).
42. Alcamí P, Pereda AE, Beyond plasticity: the dynamic impact of electrical synapses on neural circuits. Nat Rev Neurosci. 20, 253–271 (2019). [PubMed: 30824857]
43. Walker F et al. , Parvalbumin- and vasoactive intestinal polypeptide-expressing neocortical interneurons impose differential inhibition on Martinotti cells. Nat Commun. 7, 13664 (2016). [PubMed: 27897179]
44. Thomson AM, West DC, Wang Y, Bannister AP, Synaptic Connections and Small Circuits Involving Excitatory and Inhibitory Neurons in Layers 2–5 of Adult Rat and Cat Neocortex: Triple Intracellular Recordings and Biocytin Labelling In Vitro. Cereb Cortex. 12, 936–953 (2002). [PubMed: 12183393]
45. Pala A, Petersen CCH, In Vivo Measurement of Cell-Type-Specific Synaptic Connectivity and Synaptic Transmission in Layer 2/3 Mouse Barrel Cortex. Neuron. 85, 68–75 (2015). [PubMed: 25543458]
46. Jouhanneau J-S, Kremkow J, Dorrn AL, Poulet JFA, In Vivo Monosynaptic Excitatory Transmission between Layer 2 Cortical Pyramidal Neurons. Cell Reports. 13, 2098–106 (2015). [PubMed: 26670044]
47. Thomson AM, Activity-dependent properties of synaptic transmission at two classes of connections made by rat neocortical pyramidal axonsin vitro. J Physiology. 502, 131–147 (1997).
48. Beierlein M, Gibson JR, Connors BW, Two Dynamically Distinct Inhibitory Networks in Layer 4 of the Neocortex. J Neurophysiol. 90, 2987–3000 (2003). [PubMed: 12815025]
49. Ma Y, Hu H, Agmon A, Short-Term Plasticity of Unitary Inhibitory-to-Inhibitory Synapses Depends on the Presynaptic Interneuron Subtype. J Neurosci. 32, 983–988 (2012). [PubMed: 22262896]
50. Reyes A, Lujan R, Rozov A, Burnashev N, Somogyi P, Sakmann B, Target-cell-specific facilitation and depression in neocortical circuits. Nat Neurosci. 1, 279–285 (1998). [PubMed: 10195160]
51. Balaram P, Kaas JH, Towards a unified scheme of cortical lamination for primary visual cortex across primates: insights from NeuN and VGLUT2 immunoreactivity. Front Neuroanat. 8, 81 (2014). [PubMed: 25177277]
52. Berg J et al. , Human neocortical expansion involves glutamatergic neuron diversification. Nature. 598, 151–158 (2021). [PubMed: 34616067]
53. Kalmbach BE et al. , h-Channels Contribute to Divergent Intrinsic Membrane Properties of Supragranular Pyramidal Neurons in Human versus Mouse Cerebral Cortex. Neuron. 100, 1194–1208.e5 (2018). [PubMed: 30392798]
54. Bird AD, Wall MJ, Richardson MJE, Bayesian Inference of Synaptic Quantal Parameters from Correlated Vesicle Release. Front Comput Neurosc. 10, 116 (2016).
55. Barri A, Wang Y, Hansel D, Mongillo G, Eneuro, in press, doi:10.1523/eneuro.0113-15.2016.
56. Nanou E, Catterall WA, Calcium Channels, Synaptic Plasticity, and Neuropsychiatric Disease. Neuron. 98, 466–481 (2018). [PubMed: 29723500]
57. Markram H, Wang Y, Tsodyks M, Differential signaling via the same axon of neocortical pyramidal neurons. Proc National Acad Sci. 95, 5323–5328 (1998).
58. Ma Y, Hu H, Agmon A, Short-Term Plasticity of Unitary Inhibitory-to-Inhibitory Synapses Depends on the Presynaptic Interneuron Subtype. J Neurosci. 32, 983–988 (2012). [PubMed: 22262896]
59. Bykowska O et al. , Model-Based Inference of Synaptic Transmission. Frontiers Synaptic Neurosci. 11, 21 (2019).

60. Keller AJ et al. , A Disinhibitory Circuit for Contextual Modulation in Primary Visual Cortex. Neuron. 108, 1181–1193.e8 (2020). [PubMed: 33301712]
61. Fu Y et al. , A Cortical Circuit for Gain Control by Behavioral State. Cell. 156, 1139–1152 (2014). [PubMed: 24630718]
62. Millman DJ et al. , VIP interneurons in mouse primary visual cortex selectively enhance responses to weak but specific stimuli. Elife. 9, e55130 (2020). [PubMed: 33108272]
63. Dipoppa M, Ranson A, Krumin M, Pachitariu M, Carandini M, Harris KD, Vision and Locomotion Shape the Interactions between Neuron Types in Mouse Visual Cortex. Neuron. 98, 602–615.e8 (2018). [PubMed: 29656873]
64. Hu H, Ma Y, Agmon A, Submillisecond Firing Synchrony between Different Subtypes of Cortical Interneurons Connected Chemically But Not Electrically. J Neurosci. 31, 3351–3361 (2011). [PubMed: 21368047]
65. Gibson JR, Beierlein M, Connors BW, Two networks of electrically coupled inhibitory neurons in neocortex. Nature. 402, 75–79 (1999). [PubMed: 10573419]
66. Gouwens NW et al. , Integrated Morphoelectric and Transcriptomic Classification of Cortical GABAergic Cells. Cell. 183, 935–953.e19 (2020). [PubMed: 33186530]
67. Niell CM, Stryker MP, Highly selective receptive fields in mouse visual cortex. J Neurosci Official J Soc Neurosci. 28, 7520–36 (2008).
68. Almási Z, Dávid C, Witte M, Staiger JF, Distribution Patterns of Three Molecularly Defined Classes of GABAergic Neurons Across Columnar Compartments in Mouse Barrel Cortex. Front Neuroanat. 13, 45 (2019). [PubMed: 31114486]
69. Gonchar Y, Wang Q, Burkhalter AH, Multiple distinct subtypes of GABAergic neurons in mouse visual cortex identified by triple immunostaining. Front Neuroanat. 2, 3 (2008).
70. Lur G, Vinck MA, Tang L, Cardin JA, Higley MJ, Projection-Specific Visual Feature Encoding by Layer 5 Cortical Subnetworks. Cell Reports. 14, 2538–2545 (2016). [PubMed: 26972011]
71. Kim EJ, Juavinett AL, Kyubwa EM, Jacobs MW, Callaway EM, Three Types of Cortical Layer 5 Neurons That Differ in Brain-wide Connectivity and Function. Neuron. 88, 1253–1267 (2015). [PubMed: 26671462]
72. Scala F et al. , Phenotypic variation of transcriptomic cell types in mouse motor cortex. Nature, 1–7 (2020).
73. Azouz R, Gray CM, Dynamic spike threshold reveals a mechanism for synaptic coincidence detection in cortical neurons in vivo. Proc National Acad Sci. 97, 8110–8115 (2000).
74. Barnes SJ et al. , Delayed and Temporally Imprecise Neurotransmission in Reorganizing Cortical Microcircuits. J Neurosci. 35, 9024–9037 (2015). [PubMed: 26085628]
75. Obermayer J et al. , Lateral inhibition by Martinotti interneurons is facilitated by cholinergic inputs in human and mouse neocortex. Nat Commun. 9, 4101 (2018). [PubMed: 30291244]
76. Silberberg G, Markram H, Disynaptic Inhibition between Neocortical Pyramidal Cells Mediated by Martinotti Cells. Neuron. 53, 735–746 (2007). [PubMed: 17329212]
77. Gupta A, Wang Y, Markram H, Organizing Principles for a Diversity of GABAergic Interneurons and Synapses in the Neocortex. Science. 287, 273–278 (2000). [PubMed: 10634775]
78. Graybuck LT et al. , Enhancer viruses for combinatorial cell-subclass-specific labeling. Neuron. 109, 1449–1464 (2021). [PubMed: 33789083]
79. Markram H, Lübke J, Frotscher M, Roth A, Sakmann B, Physiology and anatomy of synaptic connections between thick tufted pyramidal neurones in the developing rat neocortex. J Physiology. 500, 409–440 (1997).
80. Reyes A, Sakmann B, Developmental Switch in the Short-Term Modification of Unitary EPSPs Evoked in Layer 2/3 and Layer 5 Pyramidal Neurons of Rat Neocortex. J Neurosci. 19, 3827–3835 (1999). [PubMed: 10234015]
81. Jones HC, Keep RF, Brain fluid calcium concentration and response to acute hypercalcaemia during development in the rat. J Physiology. 402, 579–593 (1988).
82. Borst GJ, The low synaptic release probability in vivo. Trends Neurosci. 33, 259–266 (2010). [PubMed: 20371122]

83. Campagnola L, Kratz MB, Manis PB, ACQ4: an open-source software platform for data acquisition and analysis in neurophysiology research. Front Neuroinform. 8, 3 (2014). [PubMed: 24523692]
84. Costa RP, Sjöström JP, van Rossum MC, Probabilistic inference of short-term synaptic plasticity in neocortical microcircuits. Front Comput Neurosc. 7, 75 (2013).
85. Tasic B et al. , Shared and distinct transcriptomic cell types across neocortical areas. Nature. 563, 72–78 (2018). [PubMed: 30382198]
86. Tasic B et al. , Adult mouse cortical cell taxonomy revealed by single cell transcriptomics. Nat Neurosci. 19, 335–346 (2016). [PubMed: 26727548]
87. Allen Cell Types Database Technical White Paper: Electrophysiology (n.d.), (available at http://help.brain-map.org/display/celltypes/Documentation).
88. Braitenberg V, Schüz A, Cortex: Statistics and Geometry of Neuronal Connectivity, 103–107 (1998).
89. Gouwens NW et al. , Classification of electrophysiological and morphological neuron types in the mouse visual cortex. Nat Neurosci. 22, 1182–1195 (2019). [PubMed: 31209381]
90. James F, Statistical Methods in Experimental Physics (World Scientific Publishing Company, ed. 2nd, 2006).
91. Wilks SS, The large-sample distribution of the likelihood ratio for testing composite hypotheses. The Annals of Mathematical Statistics. 9, 60–62 (1938).
92. Hennig MH, Theoretical models of synaptic short term plasticity. Front Comput Neurosc. 7, 45 (2013).
93. Gontier C, Pfister J-P, Identifiability of a Binomial Synapse. Front Comput Neurosc. 14, 558477 (2020).

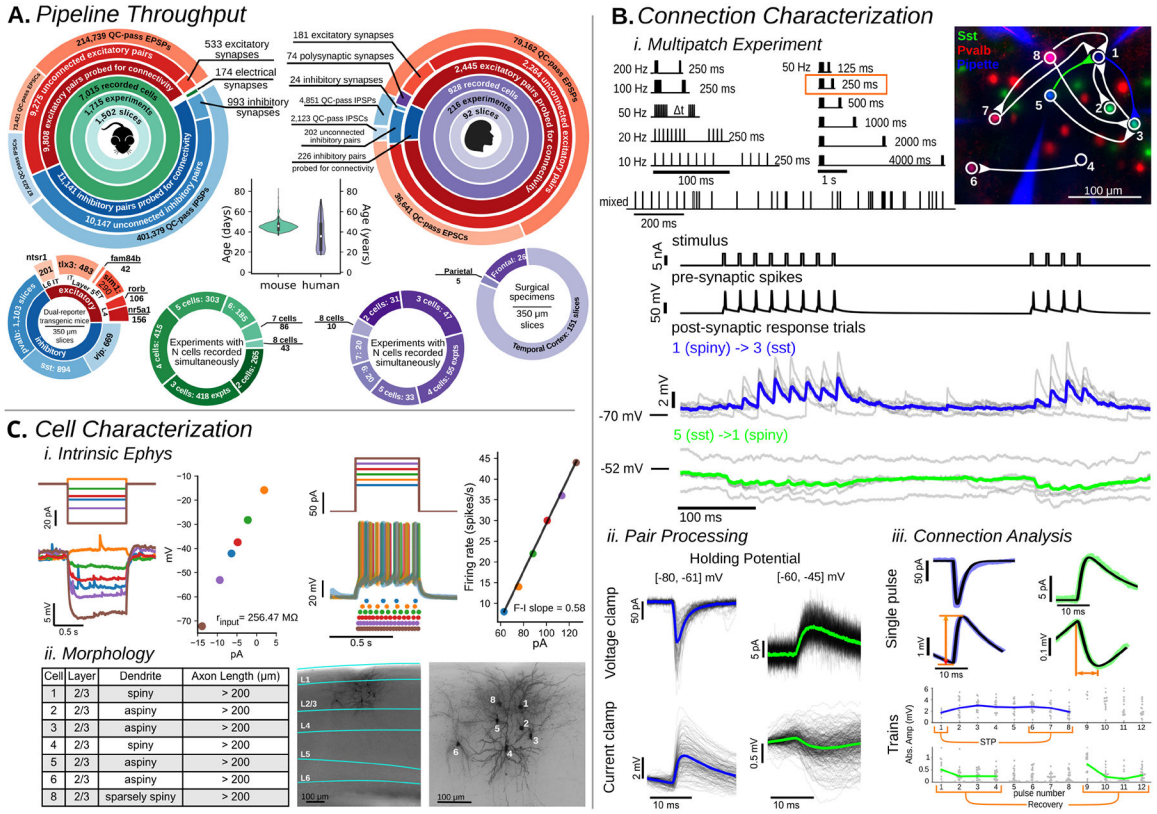

Cell	Layer	Dendrite	Axon Length (µm)
1	2/3	spiny	> 200
2	2/3	aspiny	> 200
3	2/3	aspiny	> 200
4	2/3	spiny	> 200
5	2/3	aspiny	> 200
6	2/3	aspiny	> 200
8	2/3	sparsely spiny	> 200

Fig. 1. Synaptic Physiology Pipeline:

A. Pipeline throughput summary. Large circles: data collection statistics (mouse primary visual cortex;left, human;right). Age distribution for each species (center). Distributions of recorded cells (bottom, outer circles). Experiment count with 2 through 8 simultaneously recorded cells (bottom, inner circles) B. *i.Multipatch Experiment*: Stimuli sets used to probe connectivity and dynamics (top). Fluorescent image (right) shows recorded cells with connectivity diagram overlaid. Example electrophysiology recordings of cells 1, 3, and 5 during the 50 Hz stimulus (orange box). *ii.Pair Processing*: For each recorded pair presynaptic-spike aligned postsynaptic responses (black traces) were overlaid and averaged (colored trace corresponding to the same connection in *Multipatch Experiment* panel) in both voltage clamp (top row) and current clamp (bottom row). From this a connection could be identified. *iii Connection Analysis*: When a connection was identified the average (colored) was fit (black) and metrics such as amplitude and rise time (orange lines) were extracted from the fit. Short term plasticity (STP) was quantified as a ratio from fits of individual PSPs. C. *i Intrinsic Ephys*: Long pulse steps were applied to quantify intrinsic cell properties, and electrical connections (Figure S4). Hyperpolarizing steps (left) delivered to an example cell probed the subthreshold I-V relationship to quantify metrics such as input resistance while depolarizing suprathreshold sweeps (right) were used to measure spiking and firing rate properties. *ii Morphology*: Cells were filled with biocytin during recording and stained. 20x images of the full slice stained with DAPI allowed identification of the cortical layers and 63x z-stack images were used to assess morphological properties such as dendritic type and axon length. Images and cells here are the same as in (B).

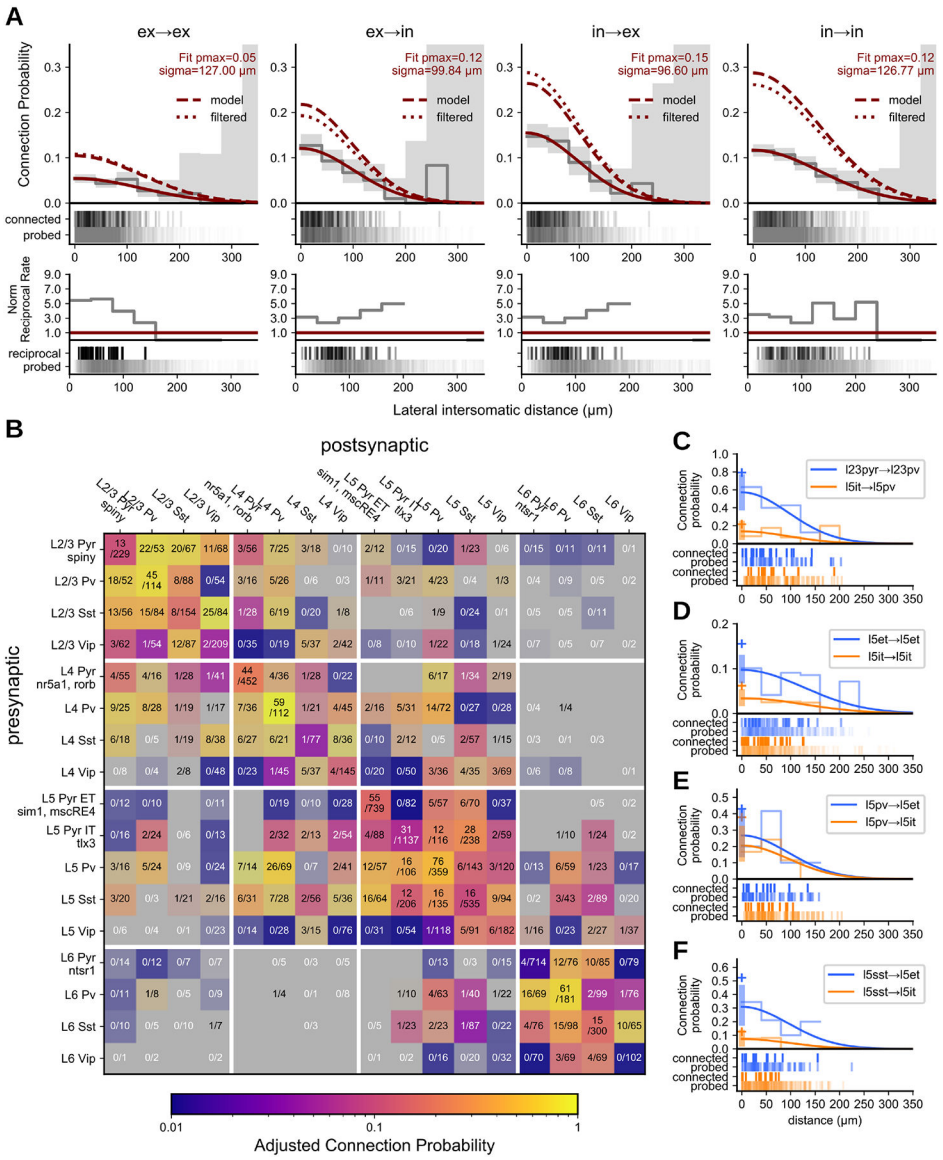

Fig. 2. Mouse Connectivity:

A. Cells were divided into two main classes, excitatory and inhibitory, and pairs classified into the four combinations of those two classes. *Top row*: Connection probability as a function of intersomatic distance fit with a Gaussian (red line) and output parameters p_{max} and sigma (σ) describe the max connection probability and width of the Gaussian. Connection probability as a function of intersomatic distance adjusted for presynaptic axon length, depth of the pair from the slice surface, and detection power of connections using a unified model (dashed red line) or via filtering of the data (dotted red line) (see Results/Methods). Grey line and area are 40 µm binned average connection probability and 95% confidence interval. Raster below shows distance distribution of connections probed (bottom) and found (top). *Bottom row*: Normalized rate of reciprocal connections. Probed pairs are unordered and the number of reciprocal connections counted was normalized to the expected value of connection probability squared for a randomly connected network (solid

red line). **B**. Connection probability matrix for mouse. Connection probability is estimated using a unified model accounting for all corrections as determined from A (dashed red line, “model”). The shading of each element indicates the 95% CI of the data with higher contrast indicating smaller CI and lower contrast (toward grey) indicating larger CI. The number of connections found out of the number of connections probed are printed in each element. **C**-**E**. Gaussian fit of connection probability vs intersomatic distance (with CI at p_{max}, shaded region) for two contrasting elements with connections found and connections probed raster below. Cross symbol denotes p_{max} with all adjustments.

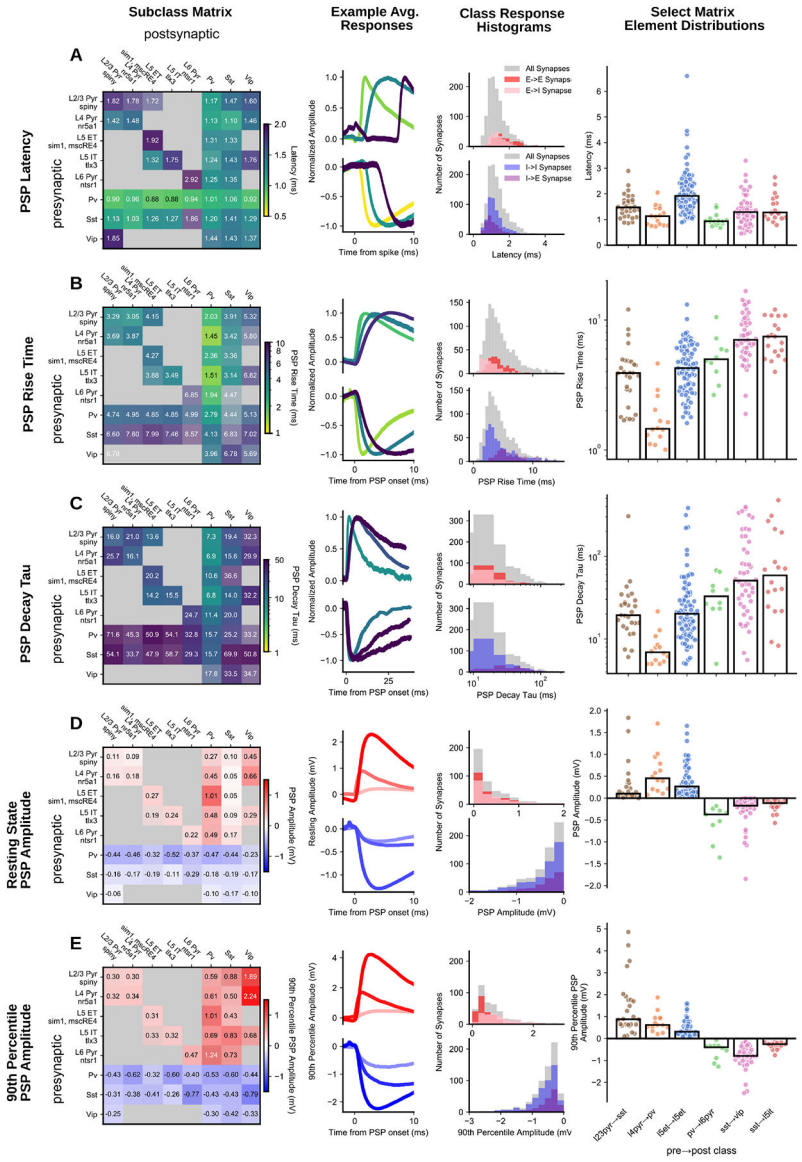

Fig 3. Synaptic strength and kinetics:

(left to right) E-I subclass matrix; excitatory and inhibitory minimum, median, and maximum average traces (light to dark colors); histograms for the major connection classes (E→E, E→I, I→I, I→E); summary scatter plots for a subset of matrix elements for each metric PSP latency **(A)**, PSP rise time **(B)**, PSP decay tau **(C)**, PSP resting state amplitude **(D)**, and PSP 90th percentile amplitude **(E)**. In all matrices, inhibitory cells are merged across layers. All matrices are colorized by the median (text in each element) with the saturation scaled by the standard error. Two or more pairs were required to fill in an element.

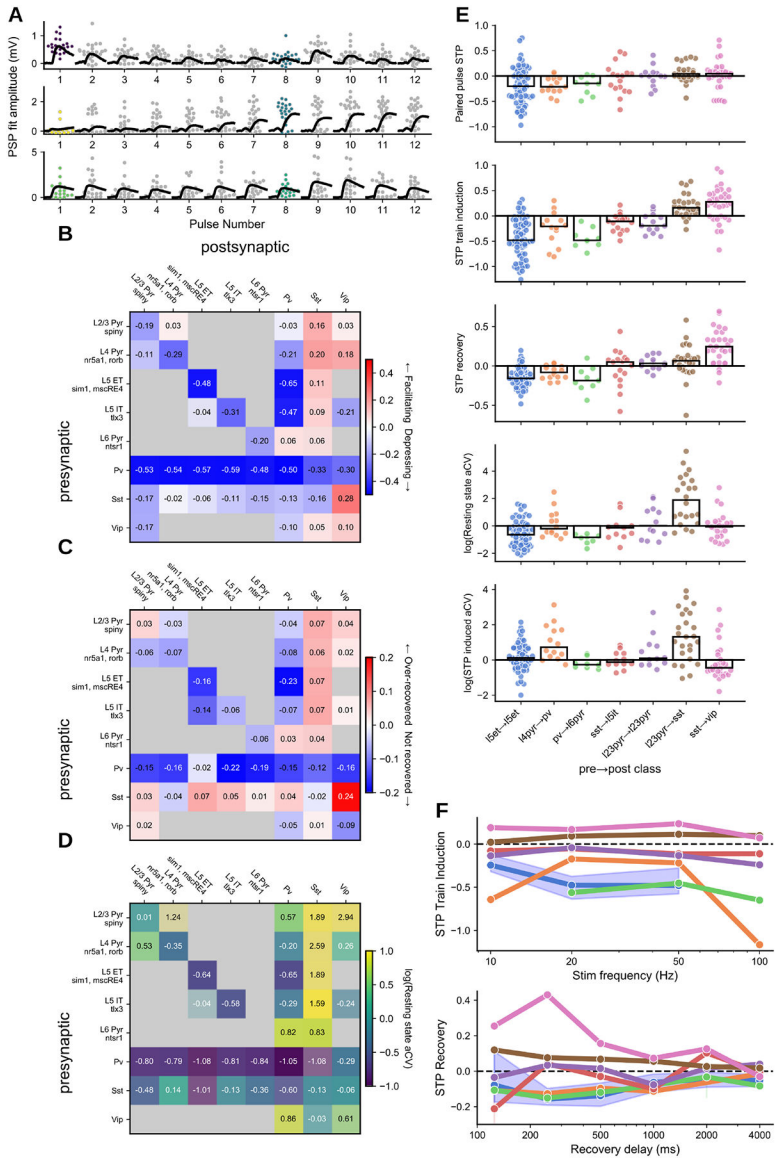

Fig 4. Synaptic dynamics:

A. Depressing, facilitating, and pseudo-linear excitatory connections (top to bottom) in 50 Hz train; grey/colored dots: individual PSP amplitudes; black traces: average PSP per pulse. Scatter points for pulse 1 (resting state aCV) and pulse 8 (STP induced aCV) are colored according to the color scale in D. B. Short-term plasticity matrix. C. Recovery (at 250ms) matrix. D. Resting state variance (adjusted coefficient of variation) matrix. All matrices are colorized by the median (text in each element) with the saturation scaled by the standard error. E. Summary plots for paired pulse ratio, STP induction ratio (avg 1st pulse amp : avg of 6th-8th pulse amp) normalized by the 90th percentile, Resting state variance, induced state variance (top to bottom). Each dot corresponds to the average response from one connection. F. Train induced STP (top) at four different frequencies (10, 20, 50, 100 Hz) for each of the elements in E (colors maintained). Each dot is the grand average of all connections in the element. For L5 ET→L5 ET the blue shading highlights the 95%

confidence interval as an example. Lower plot shows recovery from STP at six different delays (125, 250, 500, 1000, 2000, 4000 ms) in a similar manner to the plot above.

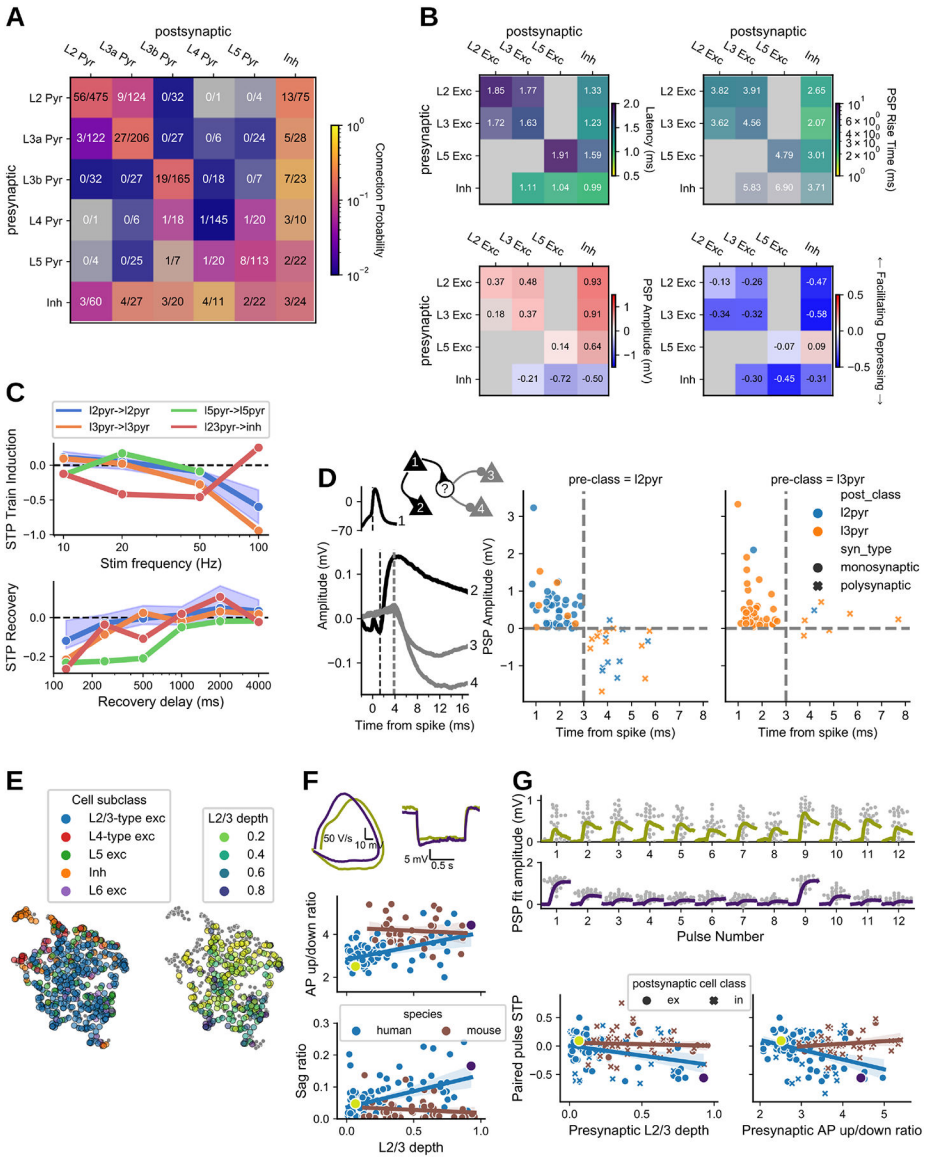

Fig 5. Human:

A. Connection probability measured from human cortical tissue. Inhibitory cells are identified by morphology as aspiny or sparsely spiny cells, grouped across layer. **B**. Kinetics, strength, and dynamics matrices are organized by layer for excitatory cells, with inhibitory cells grouped across layer. Each element is colorized by the median (text in each element) with the saturation scaled to the standard error. Two or more pairs were required to fill in an element. Latency, rise tau, and resting state amplitude are quantified from fits of the average PSP response. **C**.Train induced STP (top) across frequencies for a subset of connection types. Each dot is the median of all connections in the element, with shading for the 95% CI (bootstrapped) shown for a single example connection type. Recovery from STP at different delays (lower plot). **D**. Example polysynaptic circuit from one experiment in which cell 1 forms a short latency (~2ms) monosynaptic excitatory connection to cell 2 and delayed (~4 ms) polysynaptic inhibitory connections to cells 3 and 4 (all cells confirmed

morphologically spiny). Dashed lines indicate (from left to right) time of presynaptic spike and PSP onset. Polysynaptic connections from L2/3 pyramidal cells inferred by response latency > 3 ms vs PSP amplitude. **E**. Structure of intrinsic electrophysiology feature space. UMAP projection colored by cell subclass (left) and by depth of L2/3-type excitatory cells (right). **F**. Variation in L2/3 intrinsic properties is strongly correlated with depth in human but not mouse. Example traces show superficial and deep human cells (top, colors as in D): phase plane representation of the first spike in a depolarizing step response (left), sag in response to hyperpolarization (right). Bottom: regression of corresponding electrophysiology features vs. depth by species, with bootstrapped 95% CI. **G**. STP of L2/3 excitatory connections is structured by depth in human and not mouse. Top: PSP responses to spike trains for example cells from E. The larger response to the first spike is quantified by paired pulse STP, plotted below in relation to presynaptic depth (left) and AP up/down ratio (right) (postsynaptic relationships shown in Fig. S5E).

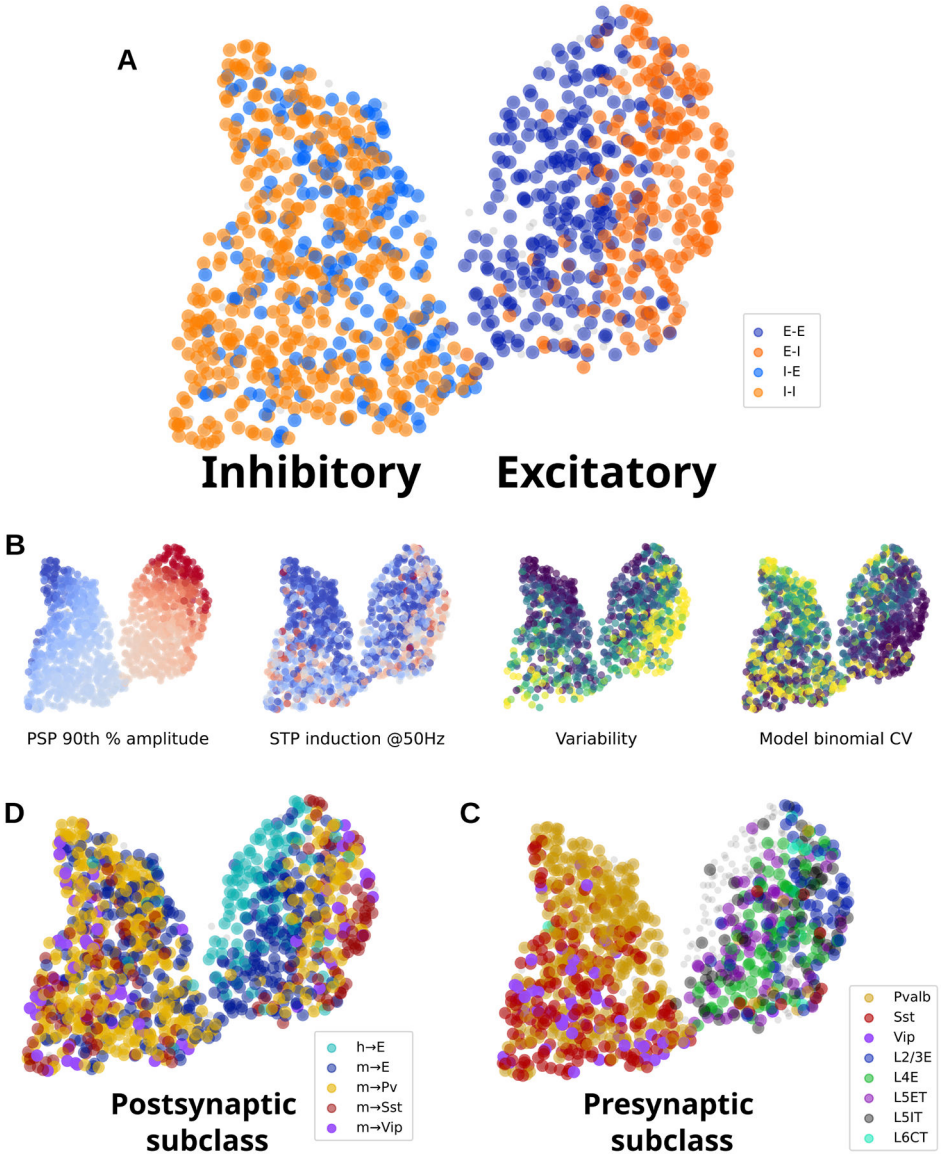

Fig 6. Dimensionality reduction on connection properties:

Relationships among connection properties and cell types revealed by dimensionality reduction. **A**. All connections colored by postsynaptic E/I cell class. The UMAP output generates two clusters: inhibitory (left) and excitatory (right). **B**. Four connection properties represented in reduced space, showing 90th percentile PSP amplitude (red=excitatory, blue=inhibitory); STP induced by 50 Hz trains (red=facilitating, blue=depressing), resting state aCV during 50 Hz trains (purple=low variability, yellow=high variability), and the binomial CV derived from model parameters (release probability * number of release sites; purple=high CV, yellow=low CV). **C**. Human and mouse connections colored by postsynaptic subclass. **D**. Mouse connections colored by presynaptic subclass.

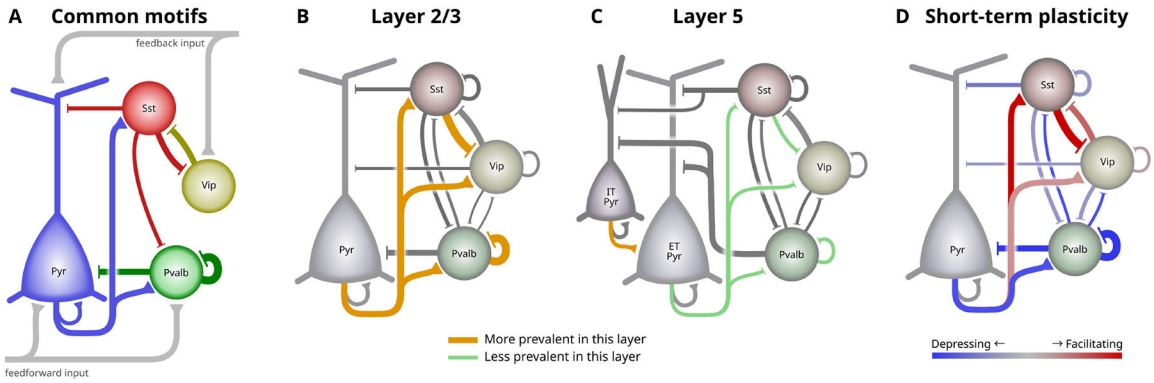

Fig 7. Intralaminar circuit diagram:

The cortical intralayer circuit differs across layer and with activity. **A**. Some commonly described elements of the intralaminar cortical circuit. Pvalb cells strongly inhibit pyramidal and other Pvalb cells, Sst cells provide broad inhibition, and Vip cells inhibit Sst cells to form a disinhibitory feedback pathway. **B-C**. Circuit diagrams showing connections between major subclasses in mouse L2/3 (B) and L5 (C). The width of connecting lines roughly represents connection probability and PSP amplitude. Connections that are prominent in each layer compared to the other are highlighted in orange, whereas green lines indicate connections that are less prevalent in that layer. For simplicity, connections between IT pyramidal and inhibitory in L5 (C) are omitted. **D**. Two complementary circuits that activate at different times. Red connections are facilitating and will be stronger during sustained activity. Blue connections are depressing and are strongest during quiescent periods.